Reaction between propargyl radical and 1,3-butadiene to form five to seven membered rings. Theoretical study

REACTION BETWEEN PROPARGYL RADICAL AND 1,3-BUTADIENE TO FORM FIVE TO SEVEN MEMBERED RINGS. THEORETICAL STUDY.

Daniela Trogolo,[1] Andrea Maranzana, Giovanni Ghigo, and Glauco Tonachini

Dipartimento di Chimica, Università di Torino, Via P. Giuria 7, I-10125 Torino, Italy

---

Abstract.

Propargyl radical addition to 1,3-butadiene seems to be a promising channel to form 5-, 6-, and 7-membered rings. These are important steps in the growth of polycyclic aromatic hydrocarbons and soot platelets. The reaction mechanism, involving 97 intermediates and 115 transition structures, was studied by CBS-QB3 method (reported here) and density functional theory. All these structures were included in the subsequent RRKM study at different combustion pressures (P=30-0.01 atm) and temperatures (T=1200-2100 K). At P=30 atm, open-chain products dominate in the whole range of temperatures. The importance of 5- and 6-membered rings rises with T, reaching a maximum in the T range 1500-1800 K. A more modest yield in 7-rings is present at T= 1500 K. At P=1 atm, in the range 1200-1500 K, the yield in 5- and 6-rings dominate. 5- and 6-rings yields are about 41% at 1200 K (CBS-QB3 data). At P=0.1 atm, 6-rings become the main products a 1000 K (35%), then they decrease to 12% (2100 K) and 5-rings rise up to 44% (1200 K), then decrease to 14% (2100 K). Open-chains are the main products at T<1000 K and T > 1500 K. Then, at P=0.01 atm, open-chain products are important below 900 K and above 1500 K,6-rings are main contributors between 900 K and 1500 K. 6-Rings reach a maximum yield of 47% (1200 K) and 5-rings 44% (1200 K) and 7-rings 17% (900 K). The main products form through to H losses.

Keywords: 1) PAH formation; 2) first C-ring; 3) propargyl; 4) 1,3-butadiene; 5) RRKM; 6) CBS-QB3; 7) Density Functional Theory

Running Title: Ring closures in propargyl + 1,3-butadiene

Corresponding authors:
e-mail: andrea.maranzana@unito.it - phone: ++39-011-6707637 - fax: ++39-011-2367637

[1] present address: Environmental Chemistry Modeling Laboratory, Swiss Federal Institute of Technology at Lausanne (EPFL), 1015 Lausanne, Switzerland.

1. Introduction

Particulate is a major contribution to the overall mass of atmospheric aerosol, and PAHs exhibit an ubiquitous presence. The impact of carbonaceous particulate[1,2] and polycyclic aromatic hydrocarbons (PAHs) on the environment is significant.[3,4] PAHs and amorphous carbon have been also identified in planetary atmospheres,[5,6] in the envelopes of carbon-rich stars,[6–9] and in the interstellar medium.[10] Graphene sheets and graphene nanoribbons are also interesting from a technological point of view.[11–15] PAHs are considered as soot precursors,[16,17] by sharing the same origin.[18–22] We have studied theoretically the growth of an aromatic system adsorbed on a model soot platelet[23] and the feasibility of van der Waals associations and σ bond formation between PAH-like molecules as a function of temperature.[24,25] Formation of aromatics, in particular the first ring, and soot particles, have been reviewed and discussed by Richter and Howard in 2000,[26] and by Frenklach in 2002.[27] The first ring formation has been studied both experimentally and computationally. Investigations have involved cyclopentene flame,[28] 1,3-butadiene + C_2[29] and C_2H[30] reactions. Bittner and Howard have suggested benzene formation via the butadienyl plus ethyne reaction.[31] Similar mechanisms (vinyl addition to ethyne, or to but-1-ene-3-yne) has also been proposed by the same groups.[32–35] Jones et al. proposed barrierless reactions of ethynyl radicals with substituted 1,3-butadiene molecule to form benzene in the interstellar medium.[36] We have previously studied[37] the first growth steps of aromatic systems through radical-breeding mechanism proposed by Krestinin,[38–40] and by radical addition of propargyl to But-1-ene-3-yne.[41]

The propargyl has been considered a species capable of generating aromatics through self-addition: recombination of two propargyl radicals can be the dominant pathway to benzene and phenyl formation.[35,42–47] It plays also an important role in the hydrocarbon growth process: for instance, the kinetics of the reaction between the propargyl radical and ethyne[48,49] and butadiyne[50,51] has been investigated both experimentally and theoretically. Similar reaction, the thermal decomposition of benzyl radical has been also computationally investigated.[52]

Butadiene has also been considered important in combustion and astrochemistry and C_2H + 1,3-butadiene reaction has also been recently investigated both theoretically and experimentally.[30]

Both the propargyl radical and 1,3-butadiene have been measured in molar fractions x, in the ranges x = 2–3 x10^{-3} and 8x10^{-5} – 6x10^{-3}, respectively.[53] They have been detected in premixed ethyne,[54] benzene,[55] toluene,[56] or gasoline[57] flames. Propargyl radical has also been detected in molar fraction up to x = 1 x 10^{-3} or 2.4 x 10^{-4} in low-pressure flames.[58,59]

In this paper we explore the possible formation of 4-, 5-, 6-, or 7-membered ring intermediates, which could be involved in subsequent PAH growth processes under combustion conditions. We simulate also the effect of four pressure values (30, 1, 0.1, and 0.01 atm): the highest pressure value could be related to internal combustion engine,[60,61] while the low pressure data could be pertinent to low-pressure flames.[59,62–68] The reacting system examined is defined by the radical addition of propargyl to 1,3-butadiene (Chart 1). ,

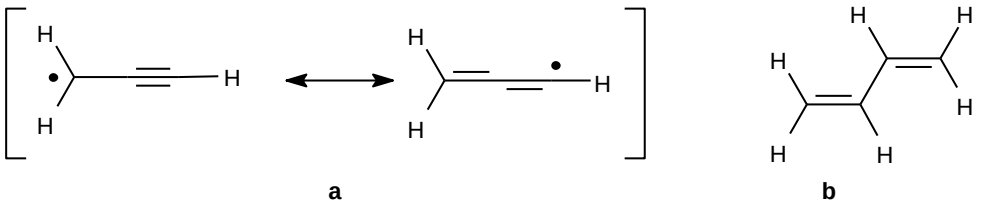

Chart 1.

2. Theoretical Method

The high-level composite method CBS-QB3[69,70] was used to study the energy hypersurface. All stationary points were determined by gradient procedures[71–75]. The nature of the minima and first order saddle points was confirmed by vibrational frequency analysis. The CBS-QB3 energies including zero point vibrational energies (ΔE_{ZPE}) are reported throughout in the text.

For comparison purpose, all the critical points were also optimized at the DFT[76] level, by using the M06-2X functional.[77–80] The cc-pVTZ basis set[81] was used in these optimizations. The optimizations were followed by cc-pVQZ[82] single-point energy calculations, to finally obtain M06-2X/CBS (complete basis set) energy estimates through the extrapolation formula put forward by Halkier et al.[83]. A validation of the computational level adopted in this study was done in a previous study.[41] The DFT energies are reported in the Supplementary Material.

Geometry optimizations and thermochemistry calculations were carried out by using the Gaussian 09 system of programs.[84]

The Rice Ramsperger Kassel Marcus (RRKM) theory,[85,86] was then used to obtain the distribution of the reaction products. In order to obtain these distributions as functions of time, RRKM and Master Equation calculations (RRKM-ME) were carried out by using the MultiWell program suite.[53,87–89] It allows to calculate sum and densities of states, then assesses micro-canonical rate constants according to RRKM theory, and finally solves the master equation. Corrections for quantum tunneling were included for all hydrogen transfer reactions (not H dissociations) by incorporating the contributions for one-dimensional

unsymmetrical Eckart barriers.[90] MultiWell stores densities and sums of states in double arrays: the lower part of the array consisted of 600 array elements, which range in energy from 0 to 2995 cm^{-1}. The higher energy part of the double array consisted of 600 elements ranging in energy from 0 to 150000 cm^{-1} with an energy spacing of 250.4 cm^{-1}. The Lennard-Jones parameters necessary for the collision frequency calculations were assumed to be the same for all the structures, and were: σ = 5.9 Å, and ε/k_B = 410 K. Energy transfer was treated by assuming the exponential-down model for collision step-size distributions: E_{down} = 2000 cm^{-1}, independent from the temperature.[52,91] This value was found to accurately reproduce the experimental falloff behavior for decomposition of benzyl radical with a good agreement between calculations and experimental data across the temperature range 300-3000K.[52]

Low-frequency modes were treated as harmonic oscillators. Rate constants were calculated in the range 1200-2100 K. In the present work, the number of stochastic trials was set to 10^7, for 300 collisions. Simulations were carried out for combustion temperatures, at different pressures (of N_2 buffer gas), namely at P = 0.01, 0.1, 1, and 30 atm, to simulate combustions under low, normal, and high[60,61] pressure conditions. Low-pressure flames are oftentimes preferred because of their nearly one dimensional structure and extended reaction zone.[59,62–68]

3. Results and discussion

3.1 Potential energy surface

Four entrance channels are conceivable: they are due to the addition of each of the external carbons (1 and 3) of the delocalized propargyl radical (a) to the positions 1 and 2 of 1,3-butadiene (b) (Chart 1). The propargyl additions to the external carbons of 1,3-butadiene have lower energy barriers compared to the additions to the internal carbons (Table 1), and the their adducts are more stable because the possibility of delocalization of the unpaired electron. Making reference to the reagents, the adducts are located at -22.1 (**1**), -6.1 (**2**), -23.1 (**3**), -7.2 (**4**) kcal mol^{-1}, respectively.

Channel	barrier	adduct
1	5.7	-22.1
2	11.1	-6.1
3	7.8	-23.1
4	13.6	-7.2

Table 1. Entrance channels: ΔE_{ZPE} (kcal mol^{-1}) barriers and adduct for the initial radical additions.

The reaction pathways that start from **1-4** are shown in Schemes 1-3. Because of the complexity of the system, the reaction mechanism (entailing 97 intermediates and 115 transition structures) has been necessarily split in three schemes, and red numbers in each scheme indicate connections to another scheme. Due to the complexity of the reaction mechanism, the numeric labels will be often mentioned not sequentially. The bold lines in Scheme 1-3 show the favorable routes leading to the most abundant products: the complete list of all the products and their yields is reported in Section 2 of the Supplementary Material. Other connections between the intermediates could be conceivable, but we arbitrarily chose to neglect transition structures with energies above 20 kcal mol^{-1} with respect to reactants.

The four initial adducts **1**-**4** are interconnected: **1** (Scheme 1) and **4** (Scheme 3) are connected through the intermediate **37**. Initial adducts **2** and **3** through structure **39** (Scheme 2). All the above-mentioned steps involve fairly moderate energies (up to 12 kcal mol^{-1} above the reactants). On the other hand, connection between **1**-**3** or **2**-**4** is much more indirect (**1**-**12**-**38**-**50**-**3** and **2**-**39**-**3**-**40**-**4**, respectively).

In Scheme 1 the most stable intermediate is the 7-ring **8** at -60.6 kcal mol^{-1} with respect to the reactants. It is formed starting from **1**, by cyclization (**5**), then ring opening (**6**) followed by another cyclization (**7**). However, the H migration **7**-**8** involves a high barrier (21.0 kcal mol^{-1}) and in case the system was thermalized, this barrier could be demanding enough to make the formation of the **8** (and **9**) difficult (see section 3.2).

Other important structures are the 5-rings due to H losses **18**, **30** and **31**. These H losses have high barriers but they are irreversible and they possibly “pump away” from the C_7H_9 system.

In Scheme 2 the most relevant structures are the 5-ring **70**, and the 6-rings **44**, **47** and **55**, formed by H losses. All the products are formed from **2** or **3**, by passing through several intermediates which, in some case, involve moderate barrier heights.

From **4** (Scheme 3), after ring closure and H loss, the most promising products are the 6-rings **47** and **87**, and the 5-rings **78** and **84**: the barrier could be fairly high (e.g. 32.6 kcal mol^{-1} for the step **46**-**47**, and 32.0 kcal mol^{-1} for **77**-**78**), but the relative energies are well below the limit of the reactants (e.g. -11.8 kcal mol^{-1} for the step **46**-**47**, and -7.4 kcal mol^{-1} for **77**-**78**).

H losses from the initial adducts lead to open-chain stable structures (**93**-**96**), characterized by high energy barriers (18-26 kcal mol^{-1} with respect to the reactants) and high exothermicity (16-24 kcal mol^{-1}), but they are favorable in terms of entropy.

The energy profile leading to the most important products, according to the RRKM (see session 3.2), are shown in Figures 1 (a-e).

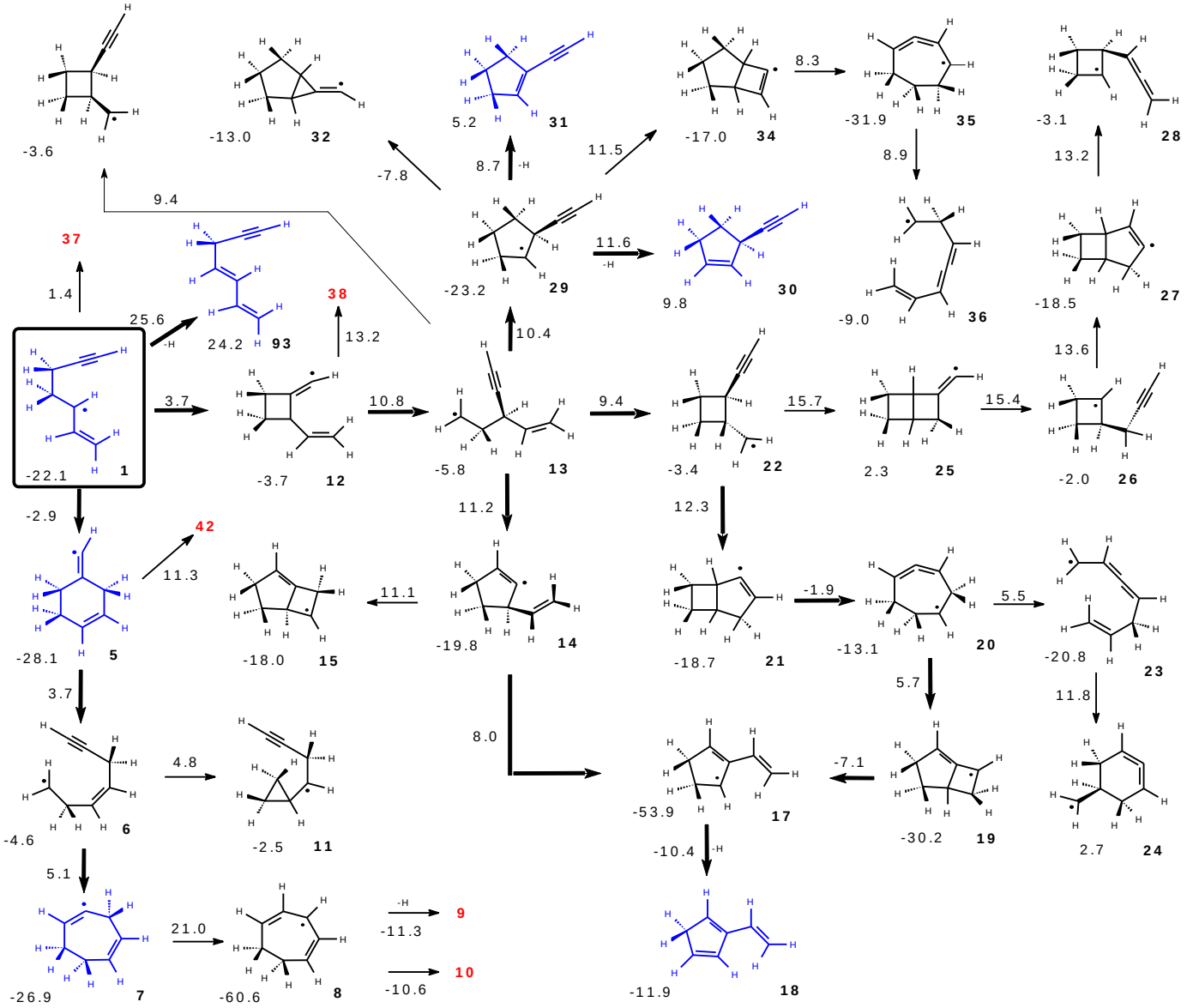

Scheme 1. Pathways toward 4-rings, 5-rings, 6-rings, and 7-rings intermediate structures that appear more promising on the basis of ΔE_{ZPE} values. The bold figures are the labels of the structures, whereas the other values are ΔE_{ZPE} energies expressed in kcal mol^{-1}. Box highlights the initial adduct **1**. The red labels are relative to structures connecting Scheme 1 to Schemes 2 and 3. The blue structures are the most abundant products, according to RRKM simulations. The bold lines show the favorable routes. The arrows do no indicate how the equilibrium is shifted, but only connections among intermediates.

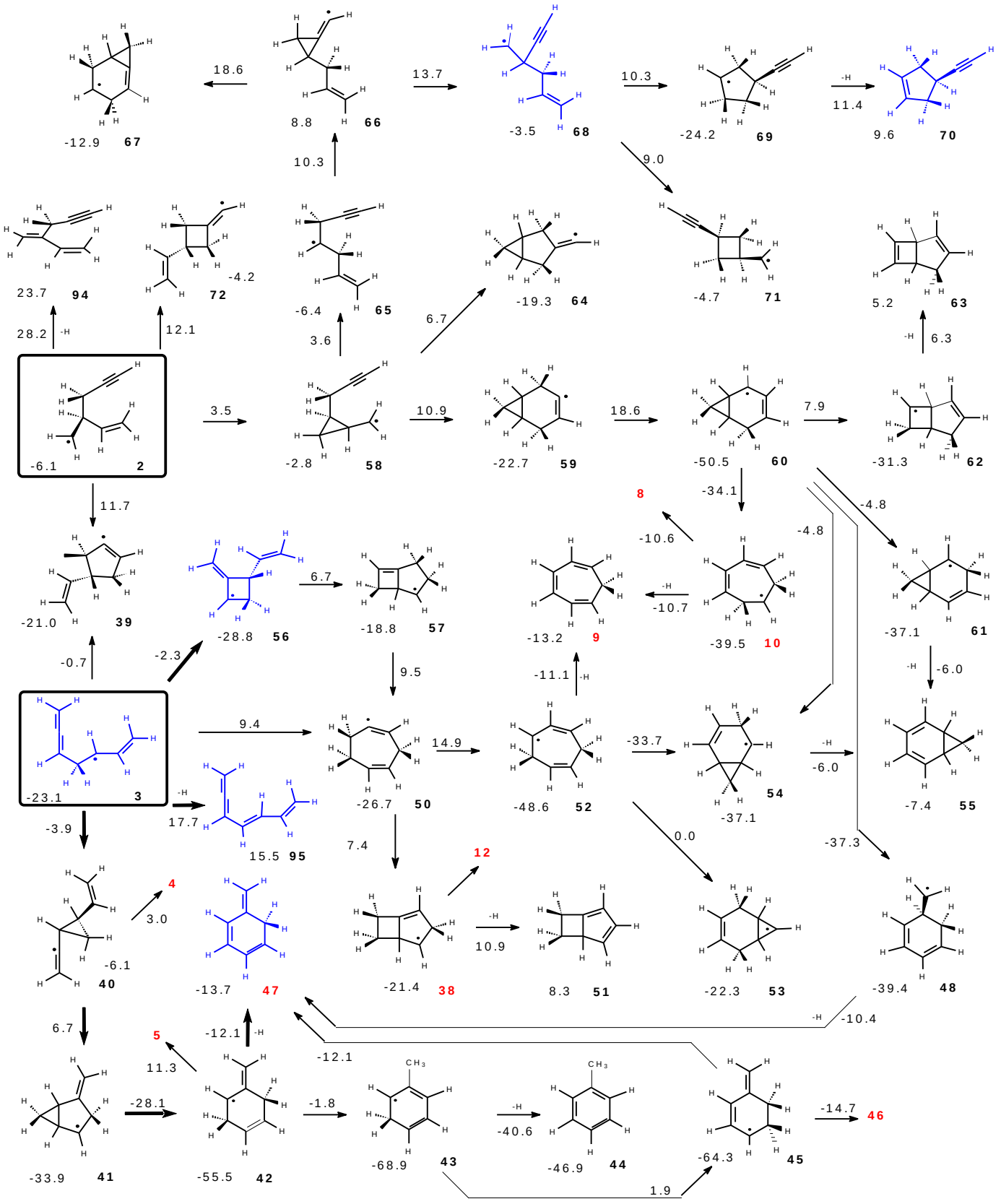

Scheme 2. Pathways toward 4-rings, 5-rings, 6-rings, and 7-rings intermediate structures that appear more promising on the basis of ΔE_{ZPE} values. The bold figures are the labels of the structures, whereas the other values are ΔE_{ZPE} energies expressed in kcal mol^{-1}. Box highlights the initial adducts **2** and **3**. The red labels are relative to structures connecting Scheme 2 to Schemes 1 and 3. The blue structures are the most abundant products, according to RRKM simulations. The bold lines show the favorable routes. The arrows do no indicate how the equilibrium is shifted, but only connections among intermediates.

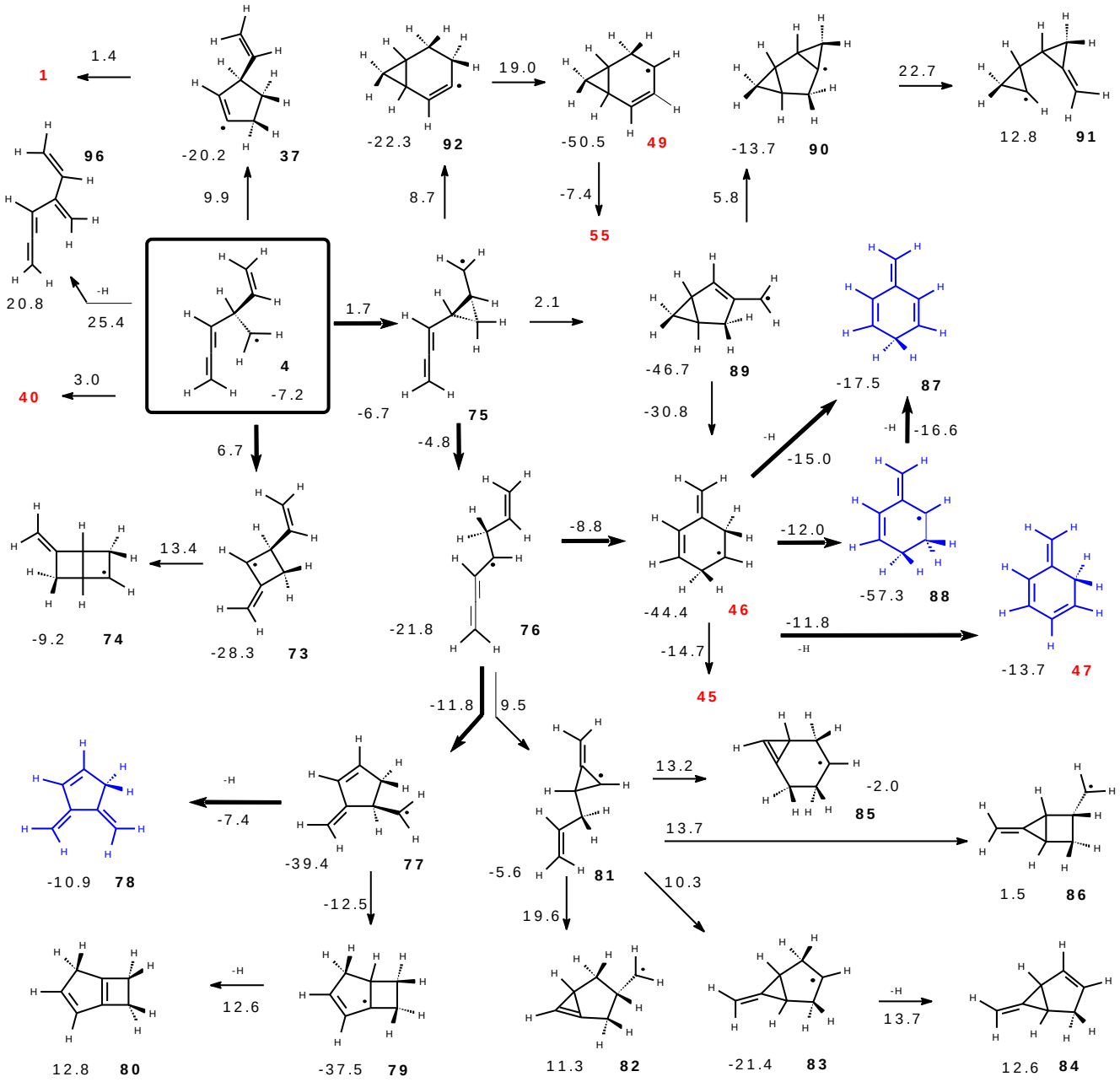

Scheme 3. Pathways toward 4-rings, 5-rings, 6-rings, and 7-rings intermediate structures that appear more promising on the basis of ΔE_{ZPE} values. The bold figures are the labels of the structures, whereas the other values are ΔE_{ZPE} energies expressed in kcal mol^{-1}. Box highlights the initial adduct **4**. The red labels are relative to structures connecting Scheme 3 to Schemes 1 and 2. The blue structures are the most abundant products, according to RRKM simulations. The bold lines show the favorable routes.The arrows do no indicate how the equilibrium is shifted, but only connections among intermediates.

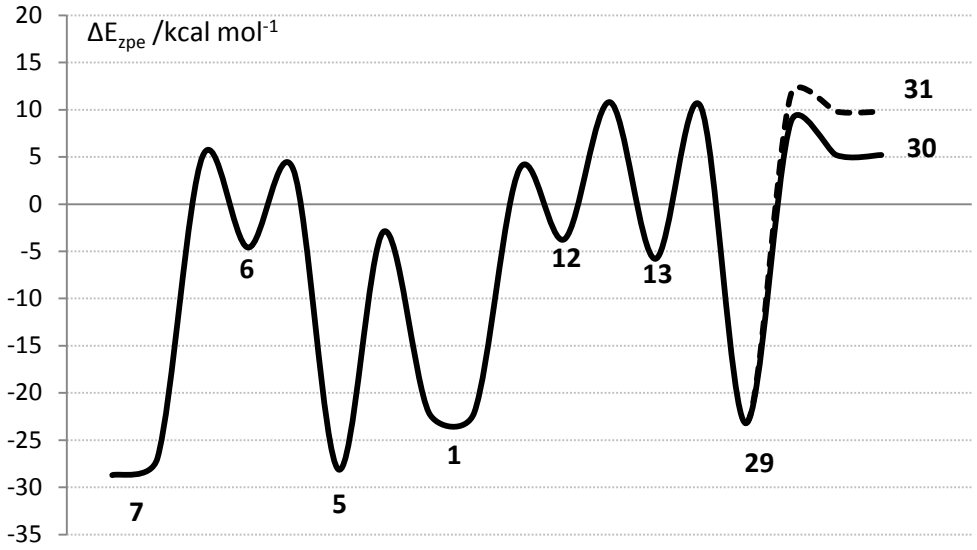
ΔE$_{zpe}$ /kcal mol^{-1}
20
15
10
5
0
-5
-10
-15
-20
-25
-30
-35
31
30
6
12
13
7
5
1
29

a

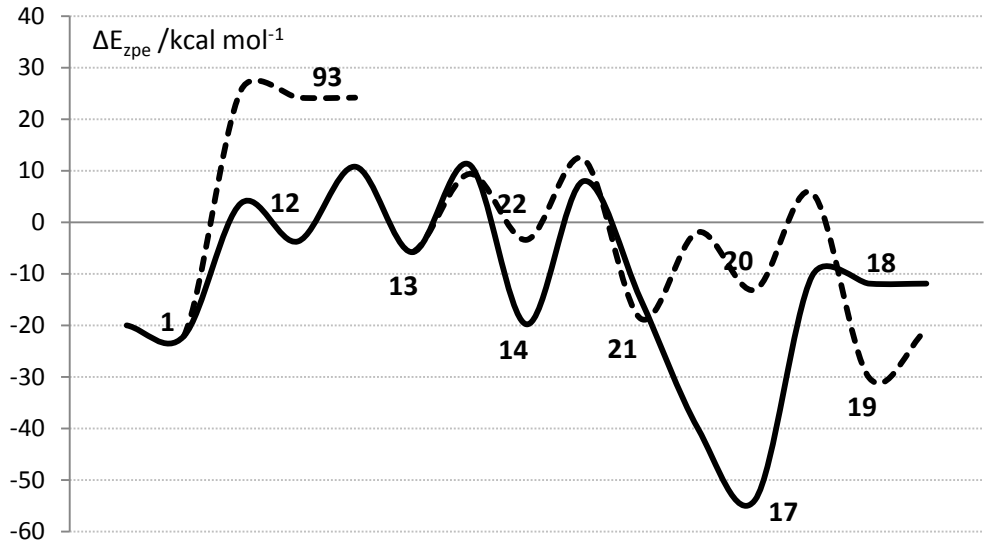
ΔE$_{zpe}$ /kcal mol^{-1}
40
30
20
10
0
-10
-20
-30
-40
-50
-60
93
12
22
20
18
1
13
14
21
19
17

b

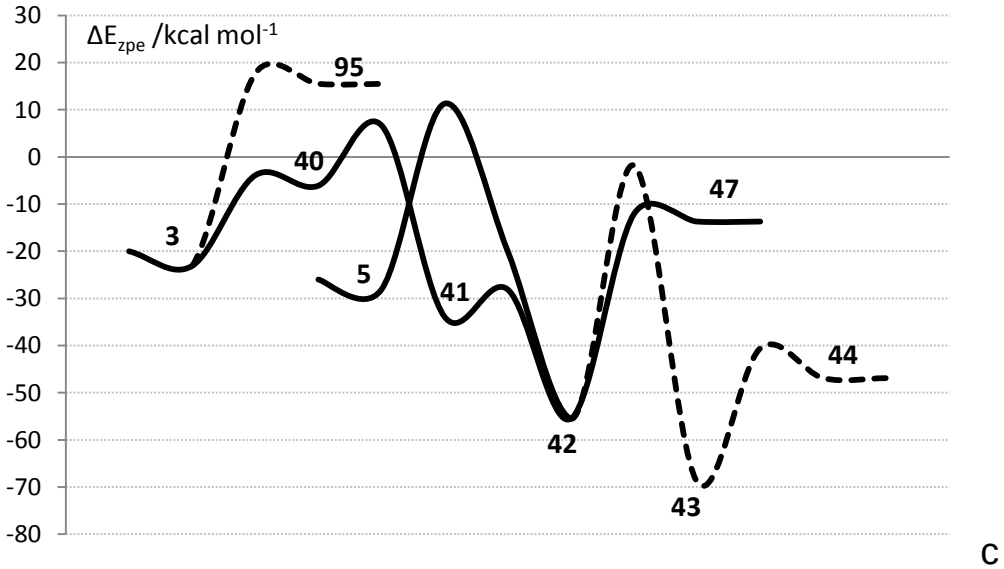
ΔE$_{zpe}$ /kcal mol^{-1}
30
20
10
0
-10
-20
-30
-40
-50
-60
-70
-80
95
40
47
3
5
41
44
42
43

c

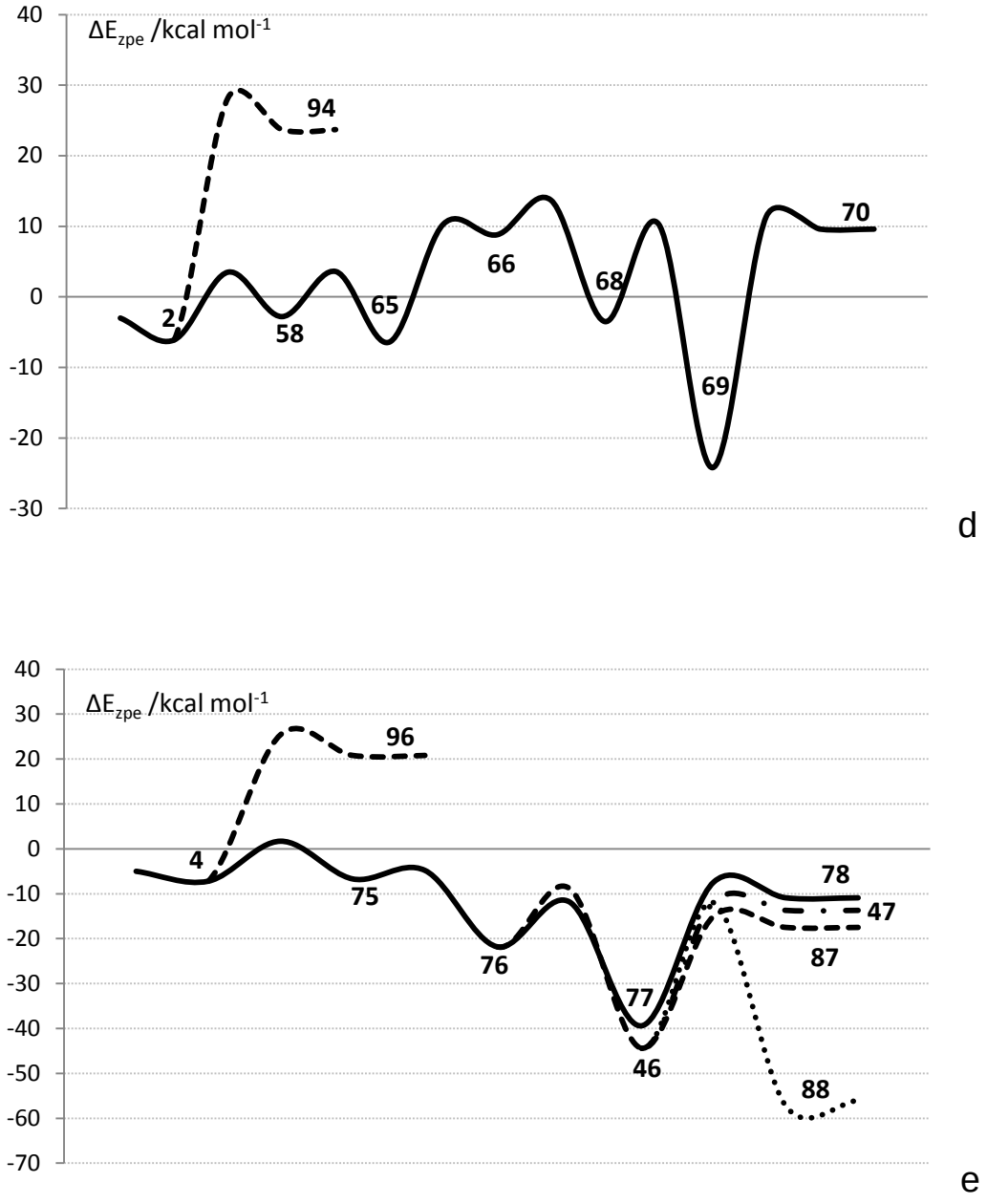

Figure 1. Pathways toward the main products. ΔE_{ZPE} values referred to the reactants (propargyl radical + 1,3-butadiene).

3.2 Master equation simulations.

The yields calculated for each of the four entrance channels (in 4 separate simulations) were scaled by the branching ratio (Section 1 of the Supplementary Material). Only for the four initial transition structures the symmetrical hindered rotation approximation was used to have a better estimate of the branching ratio. Then the total yields were calculated by summing up the four weight-averaged channels. RRKM-ME simulations show that the back-reaction to the original reactants could be significant. It more easily occurs at high temperature and low pressure. Since this effect is not observable in the experiments,

the computational results reported in this paper have been corrected for it and the net product reaction yields reported in Figure 2 exclude the re-dissociation to the initial compounds. However, for sake of clarity, the back dissociation fractions are also reported in the Figure 2, where they are referred to the same ordinate axis, but stand alone (have not to be summed up with the rest). We have estimated the net product reaction yields at four pressure values: P = 30, 1, 0.1, and 0.01 atm.

At P = 30 atm (Figure 2a), up to 1500 K, the main products are the open-chain intermediates in all the range of temperatures. Until 1500K the most abundant is **1**, followed by **3**. Above 1500K the main products are **93**, followed by **95**. The reason of this trend is a dual contribution: at low temperature the products due to the thermalization prevail; at high temperature the H losses from the initial adducts become more and more important. Plots with these two separate contributions to the open-chain yields are reported in the Section 2 of the Supplementary Material

At intermediate temperatures (1200-1500 K) the importance of 6- and 5-rings grows up to about 28 and 21% respectively, then it decreases to about 12-14% at 2100 K. The 5-rings formed are mainly **78**, but also **30**, **31**, and **18** in different ratio, depending on the temperature, whereas the 6-rings are **47**, **87**, and **5**. 4- and 7-rings formation is non-negligible only in the range 1200-1800 K: the maximum yield is ≈ 7% and 4% respectively at 1200 and 1500 K. 7-Rings are entirely constituted by the **7** intermediate. Rate constants are reported in the Section 3 of the Supplementary Material.

At P=1 atm (Figure 2b), open-chain structures are the most important contribution below T=1100 K and above 1500 K. In the intermediate range of temperatures (1100-1500 K) the yields in 5- and 6-rings dominate. The yield in 6-rings (mainly **47** and **87**, and in minor extent **5**, **45**, **88**) rises to 41% at 1200, and then decreases to 12% at 2100 K. The yield in 5-rings (**30**, **31**, and **78**) increases from 2% at 900 K to 41% at 1200 K, and then it decreases similarly to 6-rings. 7-Ring formation (**7**) is relevant only above 900 K and below 1500 K (maximum 5% at 1200 K).

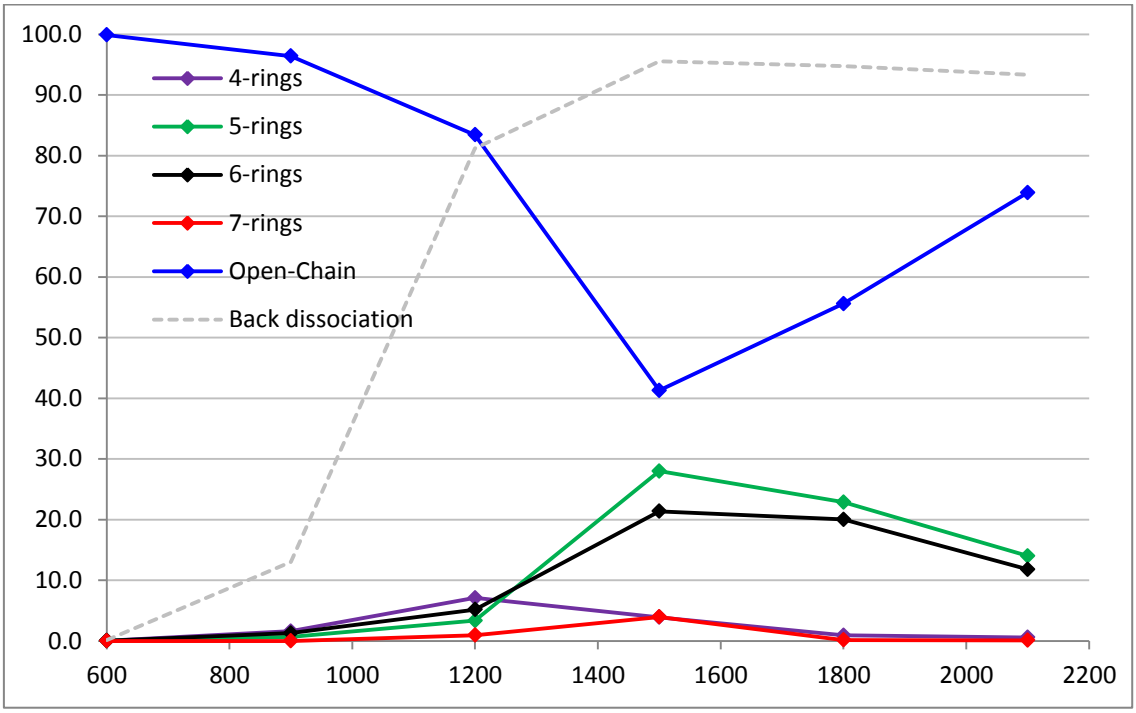
100.0
90.0
80.0
70.0
60.0
50.0
40.0
30.0
20.0
10.0
0.0
600
800
1000
1200
1400
1600
1800
2000
2200
4-rings
5-rings
6-rings
7-rings
Open-Chain
Back dissociation

a

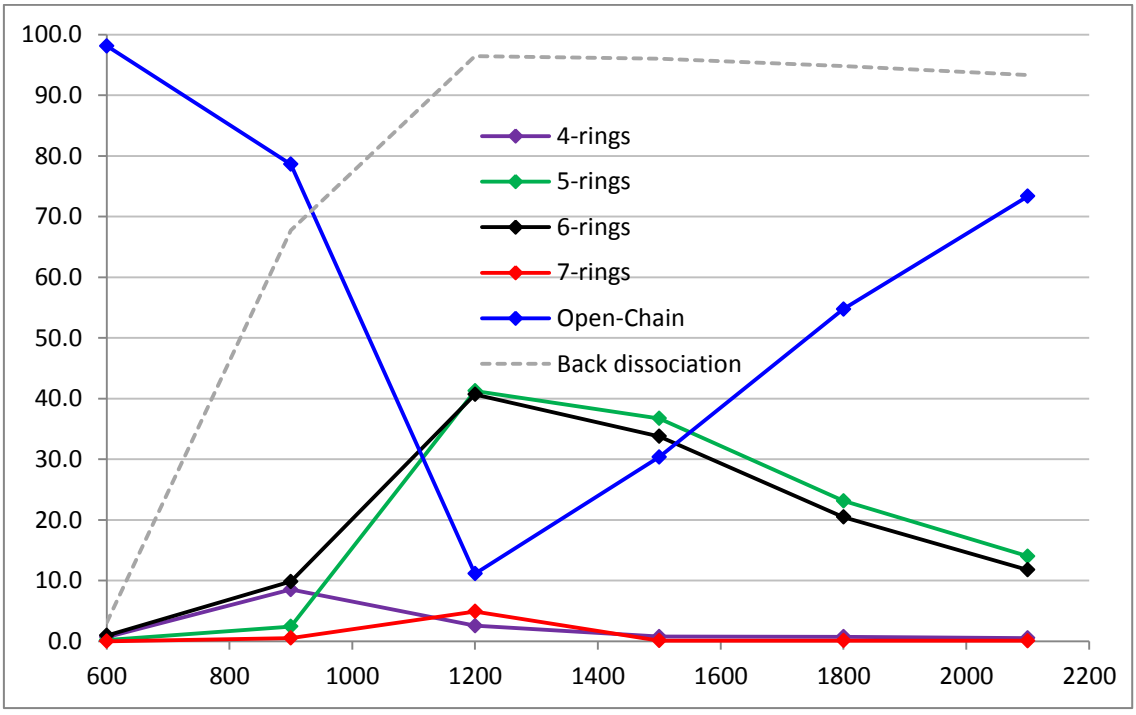
100.0
90.0
80.0
70.0
60.0
50.0
40.0
30.0
20.0
10.0
0.0
600
800
1000
1200
1400
1600
1800
2000
2200
4-rings
5-rings
6-rings
7-rings
Open-Chain
Back dissociation

b

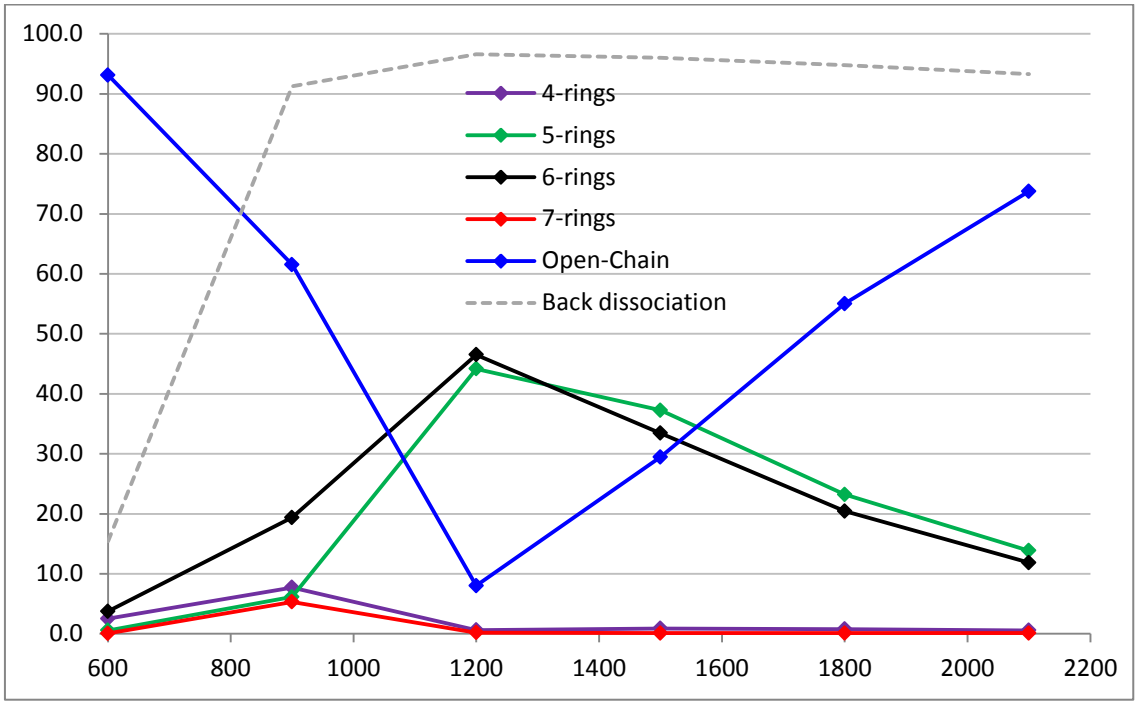

c

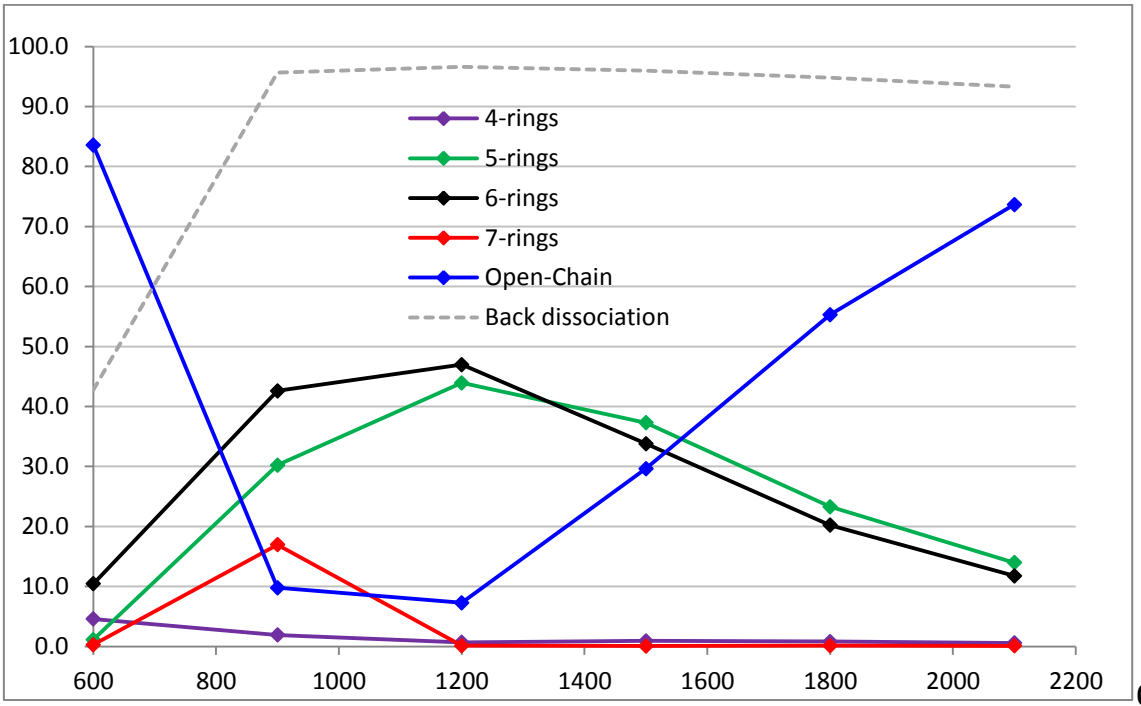

d

Figure 2. Net product reaction yields, at P = 30 atm (a), 1 atm (b), 0.1 atm (c), and 0.01 atm (d). The grey dashed lines (which stand alone) indicate the back dissociations to the reactants.

At P=0.1 atm (Figure 2c), open-chain products are important below 1100 K (**1** and **2**) and above 1500 K (**93** and **95**). The 5- and 6-rings become the main products at 1200 K: 5-ring yield reaches 44%(**30**, **31**, **78**, and **18**), and 6-ring 47% (**47**, **87**, and **45**). At higher temperatures their yields decrease to 14 and 12%, respectively (2100 K). The 4- and 7-rings contribution is below 8% over all range of T.

Then, at P=0.01 atm (Figure 2d), the behavior is similar to Figure 2c, with the exception of 7-ring (**7**), 6- and 5-rings yields which are higher at 900 K. 6-Rings become the most abundant products between 800 and 1500 K, reaching a maximum (47%) at T= 1200K. At higher T, their contribution remains important, and similar to the 5-rings contribution. The maximum 5-rings yield is 44% at T=1200 K. 7-Rings are relevant only when T is around 900 K (17%).

All the 5 and 6-rings formed during the reaction are almost exclusively products due to H loss. **7** is the only contributor to 7-rings, and **56** is the 4-ring product.

Pressure increase affects the products distribution: at lower pressure and lower temperatures the amount of open-chain products drops in favor of 5-, 6- and 7-rings formation (Figure 2). At higher temperatures they always prevail. 4-Rings yield remains below 9% in all range of temperatures and pressures.

3.3 Comparison with the DFT computations.

The 4 initial transition structures (the additions of propargyl radical to 1,3-butadiene) are 1.5-2 kcal mol^{-1} higher at M06-2X (7.2, 12.6, 9.8, 15.4 kcal mol^{-1} for **1**, **2**, **3**, and **4** formation, respectively) than at CBS-QB3 level, and the resulting rate constants are lower by a factor of 5 (600 K) to 1.2 (2100 K). Several 6-rings (**53**, **54**, **55**, **59**, **60**) and some other intermediates (**40**, **90**, **91**) are 4-9 kcal mol^{-1} more stable when calculated by the M06-2X functional. However, in general, the DFT and CBS-QB3 energies are similar: the mean-signed deviation is -0.62 kcal mol^{-1}; mean-unsigned deviation 1.82; root mean square deviation 2.32.

The products distribution, estimated by kinetic simulations, shows similar trends with temperatures and pressures, but the yields are in some cases significantly different. This gap is especially evident at low pressures (0.01 and 0.1 atm) and low temperature (900 K): at 0.01 atm the 5-rings yield drops from 30% (CBS-QB3) to 10% (M06-2X/CBS) and, specularly, the open-chain products grow from 10% (CBS-QB3) to 27% (M06-2X/CBS). Similarly, at 0.1 atm, the 6-rings yield grows from 19% (CBS-QB3) to 38% (M06-2X/CBS), with a reduction of the open-chain products from 61% to 51%.

A sensitivity analysis has been carried out on the CBS-QB3 kinetic simulation, at 0.01 atm and 900 K, by increasing by 5% the barrier heights of first steps of the reaction (**1**-**0**, **1**-**5**,**1**-**12**, **1**-**37**, **5**-**42**, **3**-**39**, **3**-**56**, **3**-**95**, **3**-**40**, **3**-**0**), one by one. Changing the barrier of the step **1**-**0** (the back dissociation) by 1.4 A, entails a variation of -108%, -94%, -23% and +224% of the 5-, 6, 7-rings and open-chain yields, respectively. Also the barrier increase of the **1**-**5** step produces large changes of the yields: +73%, -21%, -23% for 5-, 6, open-chain, respectively. For **1**-**12** and **1**-**37**, the variations are smaller, around 20%. On the other hand, the reactions from intermediate **3** do not show significant effect on the products distribution. The

discrepancies between CBS-QB3 and M06-2X kinetic simulations could be reasonably ascribed to the small differences of the energy barriers of the first reaction steps.

The M06-2X results are reported in Sections 5-8 of the Supplementary Material.

4. Conclusions

The propargyl radical and 1,3-butadiene have been detected in significant molar fractions in flames. The reaction pathways between the two molecules to form 4-, 5-, 6-, and 7-membered carbon rings under combustion conditions have been investigated first at the DFT level. These rings can be considered as precursors of larger polycyclic systems. Several pathways, leading to 4-, 5-, 6-, and 7-rings, result promising when ΔE_{ZPE} is considered.

However, a Master Equation/RRKM study, carried out at different temperatures and pressure, has shown which products are more likely formed.

The open-chain products dominate at the lower and higher temperatures. **1** and **3** are the most abundant open-chain products at low temperature, and **93** and **95** at high T. 5- and 6-membered rings show a similar behavior with T: they grow with T and prevail starting from 900-1000 K (at 0.01 atm) or 1100 K (at 1 atm) to 1500 K. 5-Rings (**18**, **30**, **31**, **78**) and 6-rings (**5**, **45**, **47**, **87**, **88**) reach a maximum yield at 1200 K (0.01, 0.1 and 1 atm) or 1500 (30 atm) then they decrease but still remaining significant to the total observed products. Most of the prevailing products form through H losses. 7-Rings (**7**) show a trend with maximum yields depending on the pressure: at 30 atm is located at 1500 K whereas at 0.01 atm is at 900 K. These yields range from 4% (30 atm) to 17% (0.01 atm). 4-Rings (**56**, and **73**) are minor products and their yields range from 5% (0.01 atm) to 9% (1 atm).

In conclusion, the propargyl radical plus 1,3-butadiene reaction seems a promising way to form cyclic carbon systems of different extension.

Acknowledgments. This work was conducted in the frame of EC FP6 NoE ACCENT and ACCENT–PLUS projects (Atmospheric Composition Change, the European NeTwork of Excellence).

Supplementary Material includes geometries, energetics, vibrational frequencies, moments of inertia of all the structures; branching ratio; product distributions and rate constants; DFT energetics and product distributions.

References

[1] N.P. Ivleva, A. Messerer, X. Yang, R. Niessner, U. Pöschl, Raman Microspectroscopic Analysis of Changes in the Chemical Structure and Reactivity of Soot in a Diesel Exhaust Aftertreatment Model System, Environ. Sci. Technol. 41 (2007) 3702–3707.

[2] J.-O. Müller, D.S. Su, R.E. Jentoft, U. Wild, R. Schlögl, Diesel Engine Exhaust Emission: Oxidative Behavior and Microstructure of Black Smoke Soot Particulate, Environ. Sci. Technol. 40 (2006) 1231–1236.

[3] W.F. Cooke, J.J.N. Wilson, A global black carbon aerosol model, J. Geophys. Res. 101 (1996) 19395.

[4] C. Liousse, J.E. Penner, C. Chuang, J.J. Walton, H. Eddleman, H. Cachier, A global three-dimensional model study of carbonaceous aerosols, J. Geophys. Res. 101 (1996) 19411.

[5] E.H. Wilson, S.K. Atreya, Chemical sources of haze formation in Titan's atmosphere, Planet. Space Sci. 51 (2003) 1017–1033.

[6] I. Cherchneff, J.R. Barker, A.G.G.M. Tielens, Polycyclic aromatic hydrocarbon optical properties and contribution to the acceleration of stellar outflows, Astrophys. J. 377 (1991) 541.

[7] J. Cernicharo, A.M. Heras, A.G.G.M. Tielens, J.R. Pardo, F. Herpin, M. Guélin, et al., Infrared Space Observatory's Discovery of C4H2, C6H2, and Benzene in CRL 618, Astrophys. J. 546 (2001) L123–L126.

[8] J. Cernicharo, The Polymerization of Acetylene, Hydrogen Cyanide, and Carbon Chains in the Neutral Layers of Carbon-rich Proto-planetary Nebulae, Astrophys. J. 608 (2004) L41–L44.

[9] I. Cherchneff, The formation of Polycyclic Aromatic Hydrocarbons in evolved circumstellar environments, EAS Publ. Ser. 46 (2011) 177–189.

[10] L.J. Allamandola, G.G.M. Tielens, J.R. Barker, Interstellar polycyclic aromatic hydrocarbons - The infrared emission bands, the excitation/emission mechanism, and the astrophysical implications, Astrophys. J. Suppl. Ser. 71 (1989) 733.

[11] D. Wei, Y. Liu, Controllable synthesis of graphene and its applications., Adv. Mater. 22 (2010) 3225–41.

[12] Y. Wang, Z. Shi, Y. Huang, Y. Ma, C. Wang, M. Chen, et al., Supercapacitor Devices Based on Graphene Materials, J. Phys. Chem. C. 113 (2009) 13103–13107.

[13] L. Al-Mashat, K. Shin, K. Kalantar-zadeh, J.D. Plessis, S.H. Han, R.W. Kojima, et al., Graphene/Polyaniline Nanocomposite for Hydrogen Sensing, J. Phys. Chem. C. 114 (2010) 16168–16173.

[14] W. Hong, H. Bai, Y. Xu, Z. Yao, Z. Gu, G. Shi, Preparation of Gold Nanoparticle/Graphene

Composites with Controlled Weight Contents and Their Application in Biosensors, J. Phys. Chem. C. 114 (2010) 1822–1826.

[15] D. Yu, L. Dai, Self-Assembled Graphene/Carbon Nanotube Hybrid Films for Supercapacitors, J. Phys. Chem. Lett. 1 (2010) 467–470.

[16] K. Siegmann, K. Sattler, H.. Siegmann, Clustering at high temperatures: carbon formation in combustion, J. Electron Spectros. Relat. Phenomena. 126 (2002) 191–202.

[17] K.-H. Homann, Fullerenes and Soot Formation— New Pathways to Large Particles in Flames, Angew. Chemie Int. Ed. 37 (1998) 2434–2451.

[18] B.J. Finlayson-Pitts, J.N. Pitts, Chemistry of the Upper and Lower Atmosphere, in: A. Press (Ed.), Chem. Up. Low. Atmos., Elsevier, 2000: pp. 436–546.

[19] H. Böhm, H. Jander, PAH formation in acetylene–benzene pyrolysis, Phys. Chem. Chem. Phys. 1 (1999) 3775–3781.

[20] E. Ledesma, Formation and fate of PAH during the pyrolysis and fuel-rich combustion of coal primary tar, Fuel. 79 (2000) 1801–1814.

[21] I. Naydenova, P.A. Vlasov, J. Warnatz, No Title, in: Proc. Eur. Combust. Meet., Louvain-la-Neuve, Belgium, 2005.

[22] C. Jäger, F. Huisken, H. Mutschke, I.L. Jansa, T. Henning, Formation of polycyclic aromatic hydrocarbons and carbonaceous solids in gas-phase condensation experiments, Astrophys. J. 696 (2009) 706–712.

[23] A. Indarto, A. Giordana, G. Ghigo, A. Maranzana, G. Tonachini, Polycyclic aromatic hydrocarbon formation mechanism in the “particle phase”. A theoretical study., Phys. Chem. Chem. Phys. 12 (2010) 9429–40.

[24] A. Giordana, A. Maranzana, G. Tonachini, Theoretical Investigation of Soot Nanoparticle Inception via Polycyclic Aromatic Hydrocarbon Coagulation (Condensation): Energetic, Structural, and Electronic Features, J. Phys. Chem. C. 115 (2011) 1732–1739.

[25] A. Giordana, A. Maranzana, G. Tonachini, Carbonaceous Nanoparticle Molecular Inception from Radical Addition and van der Waals Coagulation of Polycyclic Aromatic Hydrocarbon-Based Systems. A Theoretical Study, J. Phys. Chem. C. 115 (2011) 17237–17251.

[26] H. Richter, J.. Howard, Formation of polycyclic aromatic hydrocarbons and their growth to soot—a review of chemical reaction pathways, Prog. Energy Combust. Sci. 26 (2000) 565–608.

[27] M. Frenklach, Reaction mechanism of soot formation in flames, Phys. Chem. Chem. Phys. 4 (2002) 2028–2037.

[28] N. Hansen, T. Kasper, S.J. Klippenstein, P.R. Westmoreland, M.E. Law, C.A. Taatjes, et al., Initial steps of aromatic ring formation in a laminar premixed fuel-rich cyclopentene flame., J. Phys. Chem.

A. 111 (2007) 4081–92.

[29] F. Zhang, B. Jones, P. Maksyutenko, R.I. Kaiser, C. Chin, V. V Kislov, et al., Formation of the phenyl radical [C6H5(X(2)A1)] under single collision conditions: a crossed molecular beam and ab initio study., J. Am. Chem. Soc. 132 (2010) 2672–83.

[30] J.F. Lockyear, M. Fournier, I.R. Sims, J.-C. Guillemin, C.A. Taatjes, D.L. Osborn, et al., Formation of fulvene in the reaction of C2H with 1,3-butadiene, Int. J. Mass Spectrom. 378 (2015) 232–245.

[31] J.D. Bittner, J.B. Howard, Composition profiles and reaction mechanisms in a near-sooting premixed benzene/oxygen/argon flame, Symp. Combust. 18 (1981) 1105–1116.

[32] M. Frenklach, W.C. Gardiner, S.E. Stein, D.W. Clary, T. Yuan, Mechanism of Soot Formation in Acetylene-Oxygen Mixtures, Combust. Sci. Technol. 50 (1986) 79–115.

[33] H. Richter, J.B. Howard, Formation and consumption of single-ring aromatic hydrocarbons and their precursors in premixed acetylene, ethylene and benzene flames, Phys. Chem. Chem. Phys. 4 (2002) 2038–2055.

[34] M. Frenklach, J. Warnatz, Detailed Modeling of PAH Profiles in a Sooting Low-Pressure Acetylene Flame, Combust. Sci. Technol. 51 (1987) 265–283.

[35] P.R. Westmoreland, A.M. Dean, J.B. Howard, J.P. Longwell, Forming benzene in flames by chemically activated isomerization, J. Phys. Chem. 93 (1989) 8171–8180.

[36] B.M. Jones, F. Zhang, R.I. Kaiser, A. Jamal, A.M. Mebel, M.A. Cordiner, et al., Formation of benzene in the interstellar medium., Proc. Natl. Acad. Sci. U. S. A. 108 (2011) 452–7.

[37] A. Indarto, A. Giordana, G. Ghigo, G. Tonachini, Formation of PAHs and soot platelets: multiconfiguration theoretical study of the key step in the ring closure-radical breeding polyyne-based mechanism, J. Phys. Org. Chem. 23 (2010) 400–410.

[38] A. Krestinin, Formation of soot particles as a process involving chemical condensation of polyines, Chem. Phys. Reports. 17 (1998) 1441–1461.

[39] A.V. Krestinin, Detailed modeling of soot formation in hydrocarbon pyrolysis, Combust. Flame. 121 (2000) 513–524.

[40] A.V. Krestinin, On the mechanism of soot formation from acetylene., Chem. Phys. Reports. 13 (1994) 191–210.

[41] D. Trogolo, A. Maranzana, G. Ghigo, G. Tonachini, First ring formation by radical addition of propargyl to but-1-ene-3-yne in combustion. Theoretical study of the C7H7 radical system., J. Phys. Chem. A. 118 (2014) 427–40.

[42] J.A. Miller, S.J. Klippenstein, The Recombination of Propargyl Radicals and Other Reactions on a C 6 H 6 Potential, J. Phys. Chem. A. 107 (2003) 7783–7799.

[43] U. Alkemade, K. Homann, Formation of c6h6 isomers by recombination of propynyl in the system sodium vapor propynylhalide, Zeitschrift Fur Phys. Chemie Neue Folge. 161 (1989) 19–34.

[44] N.M. Marinov, M.J. Castaldi, C.F. Melius, W. Tsang, Aromatic and Polycyclic Aromatic Hydrocarbon Formation in a Premixed Propane Flame, Combust. Sci. Technol. 128 (1997) 295–342.

[45] D.B. Atkinson, J.W. Hudgens, Rate Coefficients for the Propargyl Radical Self-Reaction and Oxygen Addition Reaction Measured Using Ultraviolet Cavity Ring-down Spectroscopy, J. Phys. Chem. A. 103 (1999) 4242–4252.

[46] C. Rasmussen, M. Skjoth-Rasmussen, A. Jensen, P. Glarborg, Propargyl recombination: estimation of the high temperature, low pressure rate constant from flame measurements, Proc. Combust. Inst. 30 (n.d.) 1023–1031.

[47] K. Hoyermann, F. Mauß, T. Zeuch, A detailed chemical reaction mechanism for the oxidation of hydrocarbons and its application to the analysis of benzene formation in fuel-rich premixed laminar acetylene and propene flames, Phys. Chem. Chem. Phys. 6 (2004) 3824.

[48] V.D. Knyazev, I.R. Slagle, Kinetics of the Reaction between Propargyl Radical and Acetylene, J. Phys. Chem. A. 106 (2002) 5613–5617.

[49] L. V. Moskaleva, M.C. Lin, Unimolecular isomerization/decomposition of cyclopentadienyl and related bimolecular reverse process:ab initio MO/statistical theory study, J. Comput. Chem. 21 (2000) 415–425.

[50] G. da Silva, A.J. Trevitt, Chemically activated reactions on the C7H5 energy surface: propargyl + diacetylene, i-C5H3 + acetylene, and n-C5H3 + acetylene., Phys. Chem. Chem. Phys. 13 (2011) 8940–52.

[51] A. Maranzana, A. Indarto, G. Ghigo, G. Tonachini, First carbon ring closures started by the combustive radical addition of propargyl to butadiyne. A theoretical study, Combust. Flame. 160 (2013) 2333–2342.

[52] G. da Silva, J.A. Cole, J.W. Bozzelli, Thermal decomposition of the benzyl radical to fulvenallene (C7H6) + H., J. Phys. Chem. A. 113 (2009) 6111–20.

[53] Maximum mole fractions reported are: ref. 43: 8.2 x 10-5 (1,3-butadiene) and 2.1 x 10-3 (propargyl) ref. 44: 1.5 x 10-3 (1,3-butadiene) and 2.4 x 10-3 (propargyl) ref. 45: 4.2 x 10-4 (1,3-butadiene) and 2.8 x 10-3 (propargyl) ref. 46: 5.76 x 10-3 (1,3-but, (n.d.).

[54] Y. Li, L. Zhang, Z. Tian, T. Yuan, K. Zhang, B. Yang, et al., Investigation of the rich premixed laminar acetylene/oxygen/argon flame: Comprehensive flame structure and special concerns of polyynes, Proc. Combust. Inst. 32 (2009) 1293–1300.

[55] B. Yang, Y. Li, L. Wei, C. Huang, J. Wang, Z. Tian, et al., An experimental study of the premixed benzene/oxygen/argon flame with tunable synchrotron photoionization, Proc. Combust. Inst. 31 (2007) 555–563.

[56] Y. Li, L. Zhang, Z. Tian, T. Yuan, J. Wang, B. Yang, et al., Experimental Study of a Fuel-Rich

Premixed Toluene Flame at Low Pressure, Energy & Fuels. 23 (2009) 1473–1485.

[57] Y. Li, C. Huang, L. Wei, B. Yang, J. Wang, Z. Tian, et al., An Experimental Study of Rich Premixed Gasoline/O2 /Ar Flame with Tunable Synchrotron Vacuum Ultraviolet Photoionization, Energy & Fuels. 21 (2007) 1931–1941.

[58] J. Wang, U. Struckmeier, B. Yang, T.A. Cool, P. Osswald, K. Kohse-Höinghaus, et al., Isomer-specific influences on the composition of reaction intermediates in dimethyl ether/propene and ethanol/propene flame., J. Phys. Chem. A. 112 (2008) 9255–65.

[59] F. Defoeux, V. Dias, C. Renard, P.J. Van Tiggelen, J. Vandooren, Experimental investigation of the structure of a sooting premixed benzene/oxygen/argon flame burning at low pressure, Proc. Combust. Inst. 30 (2005) 1407–1415.

[60] B. Yang, P. Oßwald, Y. LI, J. Wang, L. Wei, Z. Tian, et al., Identification of combustion intermediates in isomeric fuel-rich premixed butanol–oxygen flames at low pressure, Combust. Flame. 148 (2007) 198–209.

[61] F. V. Tinaut, A. Melgar, A. Horrillo, A. Díez de la Rosa, Method for predicting the performance of an internal combustion engine fuelled by producer gas and other low heating value gases, Fuel Process. Technol. 87 (2006) 135–142.

[62] A.T. Hartlieb, B. Atakan, K. Kohse-Höinghaus, Temperature measurement in fuel-rich non-sooting low-pressure hydrocarbon flames, Appl. Phys. B Lasers Opt. 70 (2000) 435–445.

[63] A. Faccinetto, P. Desgroux, M. Ziskind, E. Therssen, C. Focsa, High-sensitivity detection of polycyclic aromatic hydrocarbons adsorbed onto soot particles using laser desorption/laser ionization/time-of-flight mass spectrometry: An approach to studying the soot inception process in low-pressure flames, Combust. Flame. 158 (2011) 227–239.

[64] P. Desgroux, X. Mercier, B. Lefort, R. Lemaire, E. Therssen, J.F. Pauwels, Soot volume fraction measurement in low-pressure methane flames by combining laser-induced incandescence and cavity ring-down spectroscopy: Effect of pressure on soot formation, Combust. Flame. 155 (2008) 289–301.

[65] X. Wu, Z. Huang, T. Yuan, K. Zhang, L. Wei, Identification of combustion intermediates in a low-pressure premixed laminar 2,5-dimethylfuran/oxygen/argon flame with tunable synchrotron photoionization, Combust. Flame. 156 (2009) 1365–1376.

[66] H. Richter, S. Granata, W.H. Green, J.B. Howard, Detailed modeling of PAH and soot formation in a laminar premixed benzene/oxygen/argon low-pressure flame, Proc. Combust. Inst. 30 (2005) 1397–1405.

[67] H. Richter, T.G. Benish, O.A. Mazyar, W.H. Green, J.B. Howard, Formation of polycyclic aromatic hydrocarbons and their radicals in a nearly sooting premixed benzene flame, Proc. Combust. Inst. 28 (2000) 2609–2618.

[68] K.J. Rensberger, J.B. Jeffries, R.A. Copeland, K. Kohse-Höinghaus, M.L. Wise, D.R. Crosley, Laser-induced fluorescence determination of temperatures in low pressure flames., Appl. Opt. 28 (1989) 3556–66.

[69] J.A. Montgomery, M.J. Frisch, J.W. Ochterski, G.A. Petersson, A complete basis set model chemistry. VI. Use of density functional geometries and frequencies, J. Chem. Phys. 110 (1999).

[70] J.A. Montgomery, M.J. Frisch, J.W. Ochterski, G.A. Petersson, A complete basis set model chemistry. VII. Use of the minimum population localization method, J. Chem. Phys. 112 (2000) 6532–6542.

[71] J.A. Pople, P.M.W. Gill, B.G. Johnson, Kohn-Sham density-functional theory within a finite basis set, Chem. Phys. Lett. 199 (1992) 557–560.

[72] H.B. Schlegel, An efficient algorithm for calculating ab initio energy gradients using s, p Cartesian Gaussians, J. Chem. Phys. 77 (1982) 3676.

[73] H.B. Schlegel, J.S. Binkley, J.A. Pople, First and second derivatives of two electron integrals over Cartesian Gaussians using Rys polynomials, J. Chem. Phys. 80 (1984) 1976.

[74] H.B. Schlegel, Optimization of equilibrium geometries and transition structures, J. Comput. Chem. 3 (1982) 214–218.

[75] H.B. Schlegel, Computational Theoretical Organic Chemistry, in: I.G. Csizmadia, R. Daudel (Eds.), Proc. NATO Adv. Study Inst., Springer Netherlands, 1981: pp. 129–159.

[76] R.G. Parr, W. Yang, Density-Functional Theory of Atoms and Molecules, in: Density-Functional Theory Atoms Mol., Oxford University Press, 1989.

[77] Y. Zhao, D.G. Truhlar, Density functionals with broad applicability in chemistry., Acc. Chem. Res. 41 (2008) 157–67.

[78] Y. Zhao, D.G. Truhlar, How well can new-generation density functionals describe the energetics of bond-dissociation reactions producing radicals?, J. Phys. Chem. A. 112 (2008) 1095–9.

[79] Y. Zhao, D.G. Truhlar, Exploring the Limit of Accuracy of the Global Hybrid Meta Density Functional for Main-Group Thermochemistry, Kinetics, and Noncovalent Interactions, J. Chem. Theory Comput. 4 (2008) 1849–1868.

[80] Y. Zhao, D.G. Truhlar, The M06 suite of density functionals for main group thermochemistry, thermochemical kinetics, noncovalent interactions, excited states, and transition elements: two new functionals and systematic testing of four M06-class functionals and 12 other function, Theor. Chem. Acc. 120 (2008) 215–241.

[81] R.A. Kendall, T.H. Dunning, R.J. Harrison, Electron affinities of the first-row atoms revisited. Systematic basis sets and wave functions, J. Chem. Phys. 96 (1992) 6796.

[82] D.E. Woon, T.H. Dunning, Gaussian basis sets for use in correlated molecular calculations. III. The atoms aluminum through argon, J. Chem. Phys. 98 (1993) 1358.

[83] A. Halkier, T. Helgaker, P. Jørgensen, W. Klopper, H. Koch, J. Olsen, et al., Basis-set convergence in correlated calculations on Ne, N2, and H2O, Chem. Phys. Lett. 286 (1998) 243–252.

[84] M.J. Frisch, G.W. Trucks, H.B. Schlegel, G.E. Scuseria, M.A. Robb, J.R. Cheeseman, et al., Gaussian 09 Revision A.02, (n.d.).

[85] K.A. Holbrook, M.J. Pilling, S.H. Robertson, Wiley: Unimolecular Reactions, 2nd Edition - Kenneth A. Holbrook, Michael J. Pilling, Struan H. Robertson, John Wiley & Sons Inc., Chichester, 1996.

[86] R.G. Gilbert, S.C. Smith, Theory of Unimolecular and Recombination Reactions, Blackwell Science Inc, 1990.

[87] MultiWell-2014.1 Software, June 2014, designed and maintained by J. R. Barker with contributors N. F. Ortiz, J. M. Preses, L. L. Lohr, A. Maranzana, P. J. Stimac, T. L. Nguyen, and T. J. Dhilip Kumar; University of Michigan, Ann Arbor, MI;, Http://aoss.engin.umich.edu/multiwell/. (n.d.).

[88] J.R. Barker, Multiple-Well, multiple-path unimolecular reaction systems. I. MultiWell computer program suite, Int. J. Chem. Kinet. 33 (2001) 232–245.

[89] J.R. Barker, Energy transfer in master equation simulations: A new approach, Int. J. Chem. Kinet. 41 (2009) 748–763.

[90] C. Eckart, The Penetration of a Potential Barrier by Electrons, Phys. Rev. 35 (1930) 1303–1309.

[91] D. Polino, C. Cavallotti, Fulvenallene decomposition kinetics., J. Phys. Chem. A. 115 (2011) 10281–9.